Journal of Materials Chemistry A

Approaching Theoretical Specific Capacity of Iron-Rich Lithium Iron Silicate Using Graphene-incorporation and Fluoride-doing

Journal:	*Journal of Materials Chemistry A*
Manuscript ID	TA-ART-11-2021-009417.R1
Article Type:	Paper
Date Submitted by the Author:	10-Jan-2022

Complete List of Authors:	Liu, Tianwei; Hunan University Liu, Yadong; Indiana University Purdue University at Indianapolis, Yu, Yikang; Purdue University, School of Mechanical Engineering; Indiana University Purdue University at Indianapolis, Ren, Yang; City University of Hong Kong Sun, Chengjun; Argonne National Laboratory Advanced Photon Source Liu, Yuzi; Argonne national Laboratory, Center for Nanoscale Materials Xu, Jiayi; Argonne National Laboratory Liu, Cong; Argonne National Laboratory, Chemical Sciences and Engineering Division Yang, Zhenzhen; Argonne National Laboratory, Chemical Science and Engineering Lu, Wenquan; Argonne National Laboratory, Fereira, Paulo; INL - International Iberian Nanotechnology Laboratory , International Iberian Nanotechnology Laboratory (INL); International Iberian Nanotechnology Laboratory (INL) Chao, Zi-Sheng; Hunan University, College of Chemistry and Chemical Engineering; Changsha University of Science & Technology, College of Materials Science and Engineering Xie, Jian; Indiana University Purdue University at Indianapolis, Department of Mechanical Engineering

ARTICLE

Approaching Theoretical Specific Capacity of Iron-Rich Lithium Iron Silicate Using Graphene-incorporation and Fluoride-doing †

Received 00th January 20xx,
Accepted 00th January 20xx

DOI: 10.1039/x0xx00000x

Tianwei Liu,[a,b,†] Yadong Liu,[b,†] Yikang Yu,[b,c] Yang Ren,[d] Chengjun Sun,[e] Yuzi Liu,[f] Jiayi Xu,[g] Cong Liu,[g] Zhenzhen Yang,[g] Wenquan Lu,[g] Paulo Ferreira,[h] Zisheng Chao,[a] and Jian Xie [*b]

The lithium iron silicate, Li_2FeSiO_4, is a promising cathode material for lithium ion batteries due to its high theoretical specific capacity, earth abundance, low cost, and environmental friendliness. The challenges for Li_2FeSiO_4 as the practical cathode material are (1) the low electronic and ionic conductivity and (2) the low discharge voltage. The approach of incorporating graphene sheets into the nanostructure of Li_2FeSiO_4 is used for dealing with the low conductivities while fluorine doping is intended to raise up the discharge voltage. The fluorine-doped and graphene-incorporated iron-rich lithium iron silicate F-LFSO/G nanomaterials were successfully synthesized using a facile/efficient hydrothermal method with excellent performance, 328.43 mAh/g at 0.1 C rate, approaching its theoritical specific capacity, 99% of 331 mAh/g. This clearly reveals that the reversible (de)lithiation of 2 Li^+ ions per F-LFSO has been realized as results of these approaches. The (de)lithiation process has been studied using in operando high energy synchrotron X-ray absorption near edge spectrum, and X-ray photoelectron spectroscopy aided by theoretical modeling, which reveals that the F doping deeply changes the O electron configuration in the F-LFSO, and consequently makes the Li^+ ions transferred easier, while the reversible redox of oxygen can be utilized to achieve high specific capacity.

1 Introduction

Olivine-structured $LiFePO_4$ is one of the most commonly used cathode materials for lithium ion batteries (LIBs) among energy storage market [1] [2]. However, considering its unsatisfying theoretical specific capacity (i.e., 175 mAh/g), similar orthosilicate-structured Li_2FeSiO_4 (LFSO), has attracted considerable attentions, owing to its high theoretical specific capacity (331 mAh/g), good stability, low-cost, abundance in earth, and environmental friendliness [3] [4] [5-7]. In analogy with $LiFePO_4$, Li_2FeSiO_4 possesses inherent weakness of low electronic and ionic conductivity, which encumbers its electrochemical performance significantly. Furthermore, a clear understanding of structure stability with extraction of two Li^+ ions from the orthosilicate structure remains a huge challenge.

To solve these issues, approaches of fabrication of nanosheets, coating of carbon-based conductive material, doping with cation and anion etc. have been explored [8] [9] [10]. Moreover, numerous strategies have been extensively investigated, such as solid-state method[11], sol-gel method [12], supercritical hydrothermal method [8] and hydrothermal method to control the nano-sheet structure of Li_2FeSiO_4 [13]. To improve the overall electronic conductivity of the electrode, some researchers even coated Li_2FeSiO_4 particles with conductive materials[10] [14]. It has been found that the inherent electronic properties of Li_2FeSiO_4 could be substantially tuned by doping with anion and cation such as N [15] [16], Cl [17] and Ti [18]. For example, cation-doping of Ti resulted in improved capacity and rate performance but could increase the material cost. Particularly, substitution of some O with F in Li_2FeSiO_4 has been widely proved as a efficacious approach to elevate the lithium insertion/extraction voltage of cathode and thus increase overall energy density of a full cell[15].

Graphene is a single-atomic layer of sp^2-bonded carbon atoms arranged in a honeycomb crystal structure [19], which provides extraordinary electrical (i.e., extremely high electric conductivity--6.29×10^7 S/cm), mechanical (i.e., fracture strength ~130 GPa), and thermal properties (i.e., 3000 W/m-K in face) [20]. The overall approach is to use fluorine doping to improve potential of Li_2FeSiO_4 during lithiation and enhance the Li^+ ion transfer while using the graphene sheets to (1) improve the electronic conductivity and to (2) stabilize the Li_2FeSiO_4 structure during charge/discharge cycles so that the specific capacity, rate capability and cycle life can be improved. In this work, a hydrothermal method was employed to control the particle size and the special morphology of iron-rich lithium iron silicate ($Li_{4-2x}Fe_xSiO_4$, $1<x<2$) due to its facile operation and mild

[a] State State Key Laboratory for Chemo/Biosensing and Chemometrics, College of Chemistry and Chemical Engineering, Hunan University, Changsha 410082, China.
[b] Department of Mechanical & Energy Engineering, Purdue School of Engineering and Technology, Indiana University-Purdue University, Indianapolis, Indiana 46202, USA. E-mail: jianxie@iupui.edu
[c] School of Mechanical Engineering, Purdue University, West Lafayette, IN, 47907, USA.
[d] Department of Physics, City University of Hong Kong, Kowloon, Hong Kong, China.
[e] X-ray Science Division, Advanced Photon Source, Argonne National Laboratory, 9700 South Cass Avenue, Lemont, Illinois 60439, USA
[f] Center for Nanoscale Materials, Argonne National Laboratory, 9700 South Cass Avenue, Lemont, Illinois 60439, USA
[g] Chemical Science and Engineering Division, Argonne National Laboratory, 9700 South Cass Avenue, Lemont, Illinois 60439, USA.
[h] Department of Mechanical Engineering, University of Texas at Austin, TX, 78712, USA
† These authors contributed equally to this work.
† Electronic supplementary information (ESI).

reaction condition. Graphene was introduced to improve the overall electronic conductivity based on the similar approach as our previous work [21]. Fluorine, an element with the highest electronegativity of 4.0, was doped into $LiFePO_4$ to elevate the discharge voltage [22]. Along this line, part of O (with electronegativity of 3.5) in lithium iron silicate was substituted by relatively higher electronegative element F to achieve a higher discharge voltage. The fluorine doped, graphene-incorporated lithium iron silicate (F-LFSO/G) has been successfully synthesized, and their electrochemical performance as well as the mechanism of (de)lithiation has been systematically investigated. In particular, the structure evolution of F-LFSO/G was studied using in-situ HEXRD and XANES. The detailed information of valances change of Fe has been obtained from the analyzing XANES data, which suggests a potential involvement of O reversible redox similar to those Li-rich cathode materials. As a result, a specific capacity as high as ~328 mAh g^{-1} has been contributed, which is the highest capacity has been ever reported for lithium iron silicate as LIBs cathode materials [23].

2 Results and discussion

2.1 Electrochemical performance

The conclusions section should come in this section at the end of the article, before the acknowledgements. The effect of incorporation of graphene on the specific capacity is shown in Fig. 1A. Comparing with the blank LFSO, the introduction of graphene significantly improved electrochemical performance (specific capacity improved by 31.65%), which is ascribed to the increased electron conductivity. [24] In addition, it has been found that F doping can further improve specific capacity (improved by additional 35.60% compared with LFSO/G). The blank LFSO can only deliver 183.98 mAh/g, corresponding to insertion/de-insertion of about 1.1 Li^+ ion into/from each orthosilicate Li_2FeSiO_4 structure. After graphene modification, as seen from Fig. 1A, the LFSO/G delivers 242.21 mAh/g, corresponding to about 1.5 Li^+ ions insertion/de-insertion. Furthermore, a specific capacity of 328.43 mAh/g has been achieved when the LFSO/G is doped with fluorine F-LFSO/G (LFSO doped with F), which gives rise to nearly 2 Li^+ ions inserted/de-inserted. The doping F into LFSO/G indeed raises up the discharge voltage, consequently, the specific capacity/energy. In addition, there is an inflection point on the discharge curve of blank LFSO, suggesting that there are two possible distinct mechanisms of Li^+ lithiation process, leading to drastic phase changes. On the other hand, there is no inflection point on the discharge curves of LFSO/G, indicating that the phase changes are quite smooth without an abrupt shift. The inflection point appears again on the discharge curve of F-LFSO/G but to much less extent of blank LFSO, which is possibly ascribed to the F substitution of O in the LFSO, causing the reduced structural stability. Moreover, the charge/discharge curve becomes more symmetric with graphene modification and F-doping LFSO, indicating that the reversibility of (de)lithiation in F-LFSO/G material has been significantly improved. Overall, from the discharge curves, the reversibility of the (de)lithiation of LFSO is in the order of LFSO/G > F-LFSO/G > blank LFSO while the specific capacity is in the order of F-LFSO/G > LFSO/G > blank LFSO.

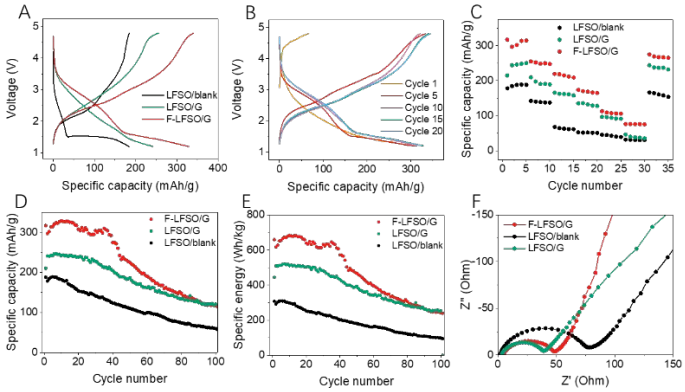

Figure 1. Electrochemical performance. (A) The best cycle charge/discharge curve comparison of LFSO/blank, LFSO/G and F-LFSO/G at 0.1C. (B) Charge/discharge curves in the initial 20 cycles of F-LFSO/G at 0.1 C at room temperature. (C) Rate performance comparison of LFSO/blank, LFSO/G and F-LFSO/G. (D) Cycle life comparison as specific capacity of LFSO/blank, LFSO/G and F-LFSO/G at 0.1C. (E) Cycle life comparison as specific energy of LFSO/blank, LFSO/G and F-LFSO/G at 0.1C. (F) Electrochemical impedance spectroscopy of LFSO/blank, LFSO/G and F-LFSO/G cells. Amplitude: 5 mV, frequency range: 1 MHz-0.01 Hz. Inset is the equivalent circuit used for fitting of impedance results.

With graphene-incorporation and fluorine-doping, the synthesized F-LFSO/G material showed the excellent electrochemical performance. The charge/discharge voltage profiles of F-LFSO/G cathode composite material at different cycle numbers at 0.1C at room temperature are shown in Fig. 1B. The 1st discharge specific capacity of this material reached 316.90 mAh/g. After a small capacity drop in the 2nd cycle, the specific capacity kept increasing in the following 15 cycles, reaching a specific capacity of 328.43 mAh/g at the 10th cycle. The achieved specific capacity of 328.43 mAh/g also suggests that nearly 2 Li^+ ions have been reversibly inserted/de-inserted into/from each orthosilicate $Li_{4-2x}Fe_xSiO_4$ structure, thus a theoretical capacity of LFSO (331 mAh/g) has been firstly approached to the best of our knowledge. In addition, at the 15th cycle, the capacity can keep at 325.96 mAh/g, and then slowly decreases (Fig. 1D). The specific capacity at 20th cycle is 306.60 mAh/g, about 93.4% of the highest specific capacity reached. Overall, the F-LFSO/G material showed high specific capacity (316.90 mAh/g) which means that a smooth insertion/extraction of 2 Li^+ ions has been achieved.

Rate performance is critical for practical application as cathode materials for Li-ion batteries. In order to understand the effect of the graphene-incorporation and fluorine-doping on the rate capability of LFSO materials, the three different LFSO materials were characterized for their rate performance. The charge/discharge rate was stepwise changed from 0.1C (16.5 mA/g) to 2C (331 mA/g) and then reversed back to 0.1C at room temperature. The doped F-LFSO/G material delivers a specific capacity of 310, 250, 210, 170, 110, 75 mAh/g, which corresponds to 100%, 80%, 67.7%, 54.8%, 35.5%, and 24.2% of the initial capacity, at the rate of 0.1C, 0.2C, 0.3C, 0.5C, 1C and 2C, respectively (Fig. 1C). The specific capacity of blank LFSO only achieves 100%, 74.47%, 32.99%, 27.13%, 23.40%, 16.49% of the initial specific capacity at the same rates. When the rate backs to 0.1C, the specific capacity returns to 268 mAh/g,

~86.5% of initial specific capacity. The rate capability of LFSO/G is between those of F-LFSO/G and LFSO blank. Overall, after the rate test, the blank LFSO and LFSO/G still keep ~88.3% and ~94.4% of the initial specific capacity while F-LFSO has ~85.9% of initial specific capacity. Both F-LFSO/G and LFSO/G show the good rate performance compared with the blank LFSO. The improved rate performance must associate with the improved electronic and ionic conductivity of these materials (see the AC impedance section).

The cycle life of these materials is shown in Fig. 1D. The specific capacity of both LFSO/blank and LFSO/G decreases with cycle number. The decay rates are 0.77%/cycle and 0.56%/cycle, respectively. However, the cycle life of F doped orthosilicate, F-LFSO/G, is slightly different. An initial capacity of 316.90 mAh/g is delivered at the 1st cycle. After the capacity drops at the 2nd cycle to 296.69 mAh/g, the specific capacity keeps increasing for more than 10 cycles, which may be ascribed to electrode activation process. At the 10th cycle, the capacity of F-LFSO/G reaches 328.43 mAh/g, the highest specific capacity achieved for this material. Then, the capacity starts to decrease until 30th cycle, then starts to raise up again to reach 310 mAh/g, decreases again all the way toward to the end of the cycle life. The cycle life of F-LFSO/G is different from those of LFSO/G and blank of LFSO. It has two bumps and after the 2nd bump, the decay rate (0.89%/cycle) is still faster than those of LSFO/G and LFSO, 0.56%/cycle and 0.77%/cycle respectively. The fast decay rate of F-LFSO/G may be associated with some structural changes of the LFSO. For the F-LSFO, two Li+ ions per F-LFSO molecule are (de)intercalated during the charge/discharge process, which the crystalline structure of F-LFSO experience much more stress from the expansion/contraction of the unit cell than those of LFSO/G and blank LSFO hosts. In addition, the substitution of F with O in LFSO may alter the redox reaction of O in the LFSO during the (de)lithiation process, which in turn, further weakens the structure of the LSFO, although the substituted F can raise up the discharge voltage. The cycling performance is also plotted as specific energy in Fig. 1E. The cycle life performance is in the order of LFSO/G > F-LFSO/G > blank LFSO, which is in consistent with that of discharge voltage.

Electrochemical impedances of LFSO/blank, LFSO/G and F-LFSO/G were measured to validate graphene sheets incorporation and F doping induced improvement of electric conductivity and Li+ ion diffusion, as shown in Fig. 1F. Obviously, the small amount of graphene in the Li_2FeSiO_4 significantly decreases the electric resistance, Re, from 74.42 Ω in $Li_{4-2x}Fe_xSiO_4$/blank to 37.52 Ω in $Li_{4-2x}Fe_xSiO_4$/G, corresponding to electronic conductivity of 2.86×10^{-8} S/cm and 5.67×10^{-8} S/cm, almost half of former. After F doping, the Re slightly increased to 44.2 Ω in F-LFSO/G compare to LFSO/G corresponding to e- conductivity of 4.43×10^{-8} S/cm, but the Li^+ ion diffusion has improved significantly. Moreover, after graphene modification, the Li^+ ion diffusion coefficient increased from 1.62×10^{-16} to 2.90×10^{-16} cm^2/s, corresponding to Li+ conductivity of 1.75×10^{-8} S/cm and 3.13×10^{-8} S/cm, nearly doubled that of blank LFSO. While with F doping, the diffusion coefficient jumped to 2.21×10^{-12} cm^2/s, and Li^+ conductivity, 2.38×10^{-4} S/cm, 4 orders of magnitude improvement, which indicates that the fluorine doping can tune the structure of LFSO and make the intercalation of Li^+ ion much easier. The strong F bonds in LFSO indeed slightly reduces the e^- conductivity but significantly increases the Li^+ conductivity. To further validate such argument, a pure F-LFSO material is prepared and tested (Fig. S1). However, those F-LFSO materials only delivers a specific capacity lower than 200 mAh/g, which is close to blank-LFSO materials (~180 mAh/g). Such results imply a one-electron reaction of LFSO-based materials without graphene incorporation. However, a fully unlock of two-electron reaction is realized with F-LFSO/G materials (~328 mAh/g), which means the F-doping has a positive effect to stabilize the two-electron reaction (O redox) but a limited effect on the one-electron reaction (Fe redox). In summary, graphene-incorporation and fluorine-doping improved the electric conductivity and solid-phase diffusion of Li ion in LFSO, thus significantly improved the electrochemical performance.

2.2 Morphology and structure characterization

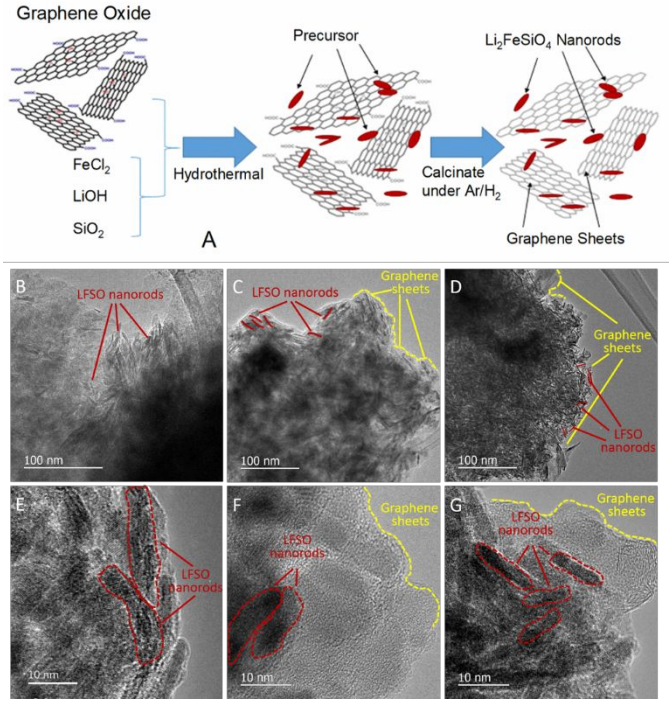

Figure 2. Schematic and Morphology. Schematic of synthesis and the 3-D structure of LFSO/G hybrid composite (A); TEM images of LFSO/blank (B, E), LFSO/G (C, F), and F-LFSO/G (D, G) at lower and higher magnifications with LFSO nanorods traced in red and graphene sheets traced in yellow, respectively.

As shown in Fig. 2A, the LFSO/G composite was prepared through a two-step method: self-assembly in the hydrothermal process and calcination in an inert atmosphere. In the hydrothermal synthesis process under high temperature and high-pressure, Li4-2xFexSiO4particles anchor on the pre-prepared graphene oxide (GO) sheets, while upon calcination, the GO sheets are reduced to graphene sheets. TEM images of the blank LFSO, LFSO/G and F-LFSO/G are shown in Fig. 2B-G, from which LFSO nanorods can be observed from all the samples. However, without the support of graphene sheets, the LFSO nanorods stack together and form large and dense chunks, as shown in Fig. (2B and E). The nanorods of graphene-incorporated LFSO/G and fluorine-doped F-LFSO/G distribute uniformly on graphene sheet as shown in Fig. 2C and F, and Fig. 2D and G, respectively. In addition, the sizes of the nanorods are

reduced after graphene-incorporation (Fig. 2C and F, indicated by red mark) and fluorine-doping (Fig. 2D and G, indicated by red dash lines encircled). Thus, the incorporated graphene sheets provide a support for $Li_{4-2x}Fe_xSiO_4$ to anchor on, leading to an excellent conductivity, while F-doping leads to the reduced particle size, which consequently reduces the diffusion distance of the Li ions and improve rate performance.

The morphology and element distribution of LFSO are examined using Scanning Electron Microscopy (SEM) and Energy Dispersive X-Ray Spectroscopy (EDX) as shown in Fig. 3A-F, and Fig. 3G, respectively. Fig. 3A reveals that for the blank LFSO, small LFSO particles stack together forming large chunks. The particle size is in the range of 0.2-5.0 µm. After graphene incorporation, the particle size is significantly reduced and a uniform distribution is realized, as shown in Fig. 3B. In addition, the LFSO particles uniformly distributed over the surface of graphene sheets (Fig. 2D and G). Fluorine doping significantly influences the morphology and particles size of LFSO. The reduced particle size certainly benefits the performance, which is confirmed by TEM (Fig. 2D and G) and electrochemical characterization results (Fig. 1).

The element distribution of these LFSO was determined using EDX. As shown in Fig.3G, all the elements are close to the ratio of precursor we used. The carbon of 8.58 wt.% is from the graphene. The atomic ratio of Fe:Si:O, 2.1:1.1:4.5, is close to the XRD result in Fig. 3F ($Fe_2(SiO_4)$), suggesting an iron-rich structure ($Li_{4-2x}Fe_xSiO_4$). In addition, the F/O atomic ratio is about 6.27%, which agrees well with the calculated percentage (6.00%).

2.3 Structural evolution during the cycling

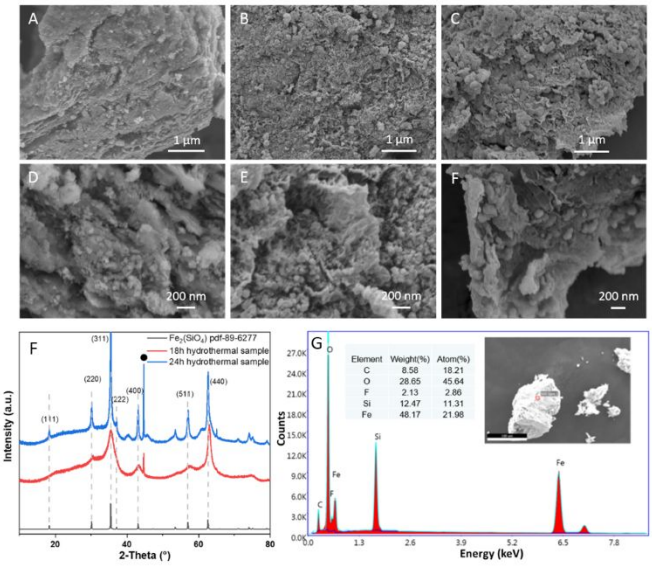

Figure 3. Pristine Structure and Composition. SEM images of LFSO/blank (A, D), LFSO/G (B, E) and F-LFSO/G (C, F) at lower and higher magnifications. (F) Powder XRD pattern of F-LFSO/G at different hydrothermal time (18h and 24h) compare to standard pattern of Fe2(SiO4) pdf-89-6277; (G) Energy-dispersive X-ray spectroscopy (EDS) of F-LFSO/G.

In order to understand the effect of the graphene incorporation and fluorine-doping on the (de)lithiation of the LFSO/G, the structures of the as-synthesized and modified LFSO samples were characterized using synchrotron high resolution X-ray diffraction shown in Fig. 3F. Comparing to the standard spectrum of $Fe_2(SiO_4)$ (pdf-89-6277), the (311), (400) and (440) peaks appeared in our F-LFSO/G sample after 18 h hydrothermal treatment. After 24 h hydrothermal treatment, the (111), (220) and (511) also appeared. All these peaks match those of standard $Fe_2(SiO_4)$. However, as marked in Fig. 3A, there is an impurity peak around 44.7° (2-Theta), which is the (110) peak of iron with the body-centred-cubic structure. The weight fraction of iron is about 4 wt. % according to the Rietveld refinement analysis of our XRD results.

It was observed that the specific capacity of F-LFSO/G changed with cycle life, showing a bell-shape between 0-40 cycles (Fig. 1E). To understand this phenomenon, where the specific capacity almost reached the theoretical specific capacity, XRD analysis of the F-LFSO/G was carried out, as shown in Fig. 4. Fig. 4B is the ex-situ XRD result after being transferred to d Space. These results show that all the peak positions almost have no shift in the first 20 cycles, but the intensity and the d-spacing change upon cycling. Comparing the crystallite size with the specific capacity, for the first 20 cycles, the crystallite size in the direction perpendicular to the lattice plane (311) shows almost no change (4.2~4.5 nm, Fig. 4C), while the crystallite size in the direction perpendicular to the lattice plane (440) also shows only small fluctuations for the first 20 cycles (>10 nm, Fig. 4D), suggesting that the structure of the material is stable with the initial Li^+ intercalation/deintercalation cycles. The crystallite size in the direction perpendicular to both planes (331 and 440) have the similar trend as the specific capacity with the cycle numbers, suggesting that the average crystal particle size changed with cycling gradually. The increased particle size seems have adversarial effect on Li+ diffusion within LFSO. After 100 cycles, crystallite size in the direction perpendicular to both plane (311) and plane (440) changed significantly, down to 0.98 nm (77.7% drop) and 6.99 nm (39.2% drop), respectively. Coincidentally, the specific capacity dropped from 320 mAh/g to 120 mAh/g. All these structural evidences indicate that a smaller grain size has been formed (pulverization) after 100 cycles, which leads to a reduction of crystalline degree of LFSO, indicated by the broadened peaks as shown in Fig. 4B. Given this situation, the reduction of ordered orthosilicate structure may further exacerbate the smooth insertion/extraction of Li ions thus contributes a reduced capacity.

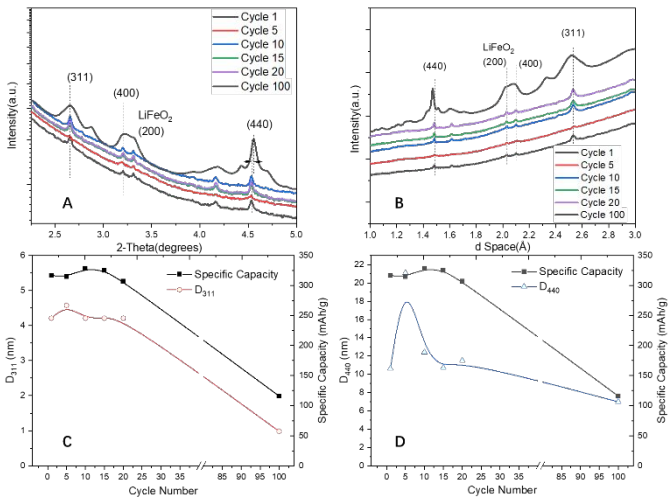

Figure 4. High resolution synchrotron XRD characterization. (A) XRD patterns of F-LFSO/G at different cycle number, (B) d Space (Å) of F-LFSO/G calculated from (A). (C) Crystallite size in the direction perpendicular to the lattice plane (311) and specific capacity at different cycles and (D) crystallite size in the direction perpendicular to the lattice plane (440) and specific capacity at different cycles.

The in-situ high energy synchrotron XRD was used to characterize F-LFSO/G cathode in a coin cell consisting of F-LFSO/G cathode and Li metal anode during charge/discharge cycle to investigate the structure change. As can be seen in Fig. 5B, the peak position (around 4.5 degrees of 2-Theta) of $Fe_2(SiO_4)$ lattice plane of (440) changes with the state of charge (SOC) during the charge/discharge process while the corresponding d spacing (Fig. 4C and D) change as well, indicating the contraction and expansion of the unit cell during the charge and discharge process respectively. The peak shifting with SOC matches well with the cell voltage change with SOC, and the curve of the peak shifting with SOC is symmetric along the charge/discharge curve (Fig. 5C), suggesting that the reversible (de)lithiation process of the F-LFSO/G is achieved [25].

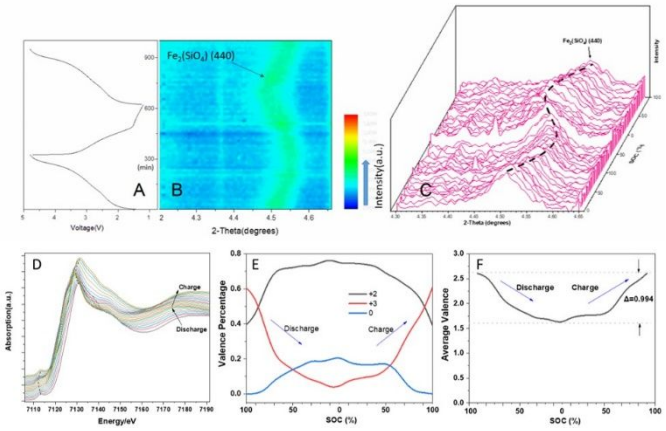

Figure 5. In situ XRD and XAS Characterizations. (A) Discharge and charge curve. (B) In-situ XRD characterization of F-LFSO/G coin cell during the 30th charge/discharge cycling at 0.1C. (C) Curve of the $Fe_2(SiO_4)$ (440) peak shifting with SOC. (D) Fe Pre-edge spectra trend in operando XAS characterization of F-LFSO/G coin cell during the second discharge/charge cycling at 0.1C. (E) Different Fe valence (Fe^0, Fe^{2+}, Fe^{3+}) percentage change when discharge and charge. (F) Average Fe valence change when discharge and charge.

The in-operando X-ray Absorption Near Edge Structure (XANES) characterization was carried out to investigate the valance change of Fe in F-LFSO/G during the (de)lithiation process. The pre-edge spectra results are shown in Fig. 5D, from which it can be seen that the Fe K-edge spectra peak change shows the clear trend (the peak shifts to higher degrees with charging process, while shifts to lower degrees with discharging process) corresponding to the discharge/charge curve at 0.1C as shown in Fig. 5A. The percentage of different valances of Fe and Fe average valance in F-LFSO/G were fitted and calculated from the spectrum. The initial F-LFSO/G has 60% Fe^{3+} and 40% Fe^{2+} (Fig. 5E). During the 1st discharge process, the Fe^{2+} content quickly increases to 70% at around 70% SOC and stays around 70% at the end of discharge (lithiation). Then, Fe^{2+} content slowly decreases to 40% (the starting content of Fe^{2+}) at the end of charge (delithiation) process. The Fe^{3+} content decreases to almost 0% at 0% SOC during the first discharge process, and then, increases from 0% to 60% at the end of charge process (100% SOC). Surprisingly, Fe0 appears at around 20% depth of discharge (DOD) or 80% SOC, and keep increasing up to ~20% until the end of discharge during the 1st discharge process, then, during the following charge process, Fe^0 content keeps steady around 20% and slightly drops to 17% until 50% SOC, and decreases to zero at 0% SOC (Fig. 5E). Based on these results from Fig. 3A, after deep discharge/charge, the Fe0 might be transferred to $LiFeO_2$, suggesting that not only intercalation is involved but also the conversion may be involved in the charge/discharge process, even it is small extent, around 17% at the most. The appearance of iron metal (Fe^0) may be one of the causes of the capacity decay of the LFSO after 40 cycles. Moreover, the XAS is also able to explain the abnormal initial Coulombic efficiency (>300%) of our LFSO based materials (Fig. 1B). The Fe-excess situation makes that there is little Li could be extracted at the first cycle which leads to a final product of Fe_xSiO_4 (1<x<2). However, in the following discharge process, there is Fe^0 involved as confirmed by XAS characterization. Such reaction makes about 2 Li intercalation and extraction in following cycles and the Coulombic efficiency returns to normal value (>97%).

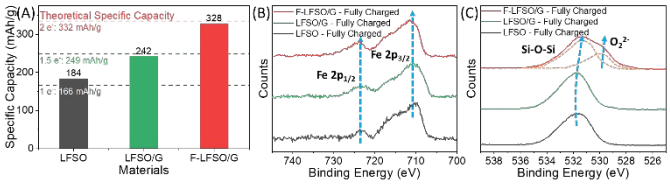

Figure 6. XPS Characterization. (A) Specific capacity comparison with theoretical capacity; (B) Fully charged Fe 2p XPS spectra comparison; (C) Fully charged O 1s spectra comparison.

The Fe average valence of F-LFSO/G decreases as the discharge proceeds until 0% SOC, then, increases with discharge and finally backs to around 2.4 close to the starting point. The average valence change is about 1.04, corresponding to $Fe^{3+} + e^- \rightarrow Fe^{2+}$ (discharge) and $Fe^{2+} \rightarrow Fe^{3+} + e^-$ (charge). However, the two valence change of Fe in F-LFSO/G was not found in the discharge/charge of F-LFSO from the XANES analysis, which does not match the charge change (2 e^- per F-LFSO molecule) involved in the discharge/charge process. The only reasonable explanation is that the reversible redox process of O might be involved as shown below.

$$Fe - 2e^- \rightarrow Fe^{2+}$$
$$Fe^{2+} - e^- \rightarrow Fe^{3+}$$
$$2O^{2-} - 2e^- \rightarrow O_2^{2-}$$

F doping has been reported that was able to stabilize the capacity decay by suppressing structural amorphization and void formation at particle surface in Li-rich cathode materials[26]. Moreover, the compositions formed by Li-binding with fluorine are stable against phase separation, thus reducing the oxygen loss during cycling[27]. Hence, it is highly possible that the F doping significantly changes the O bonding structure and helped to achieve reversible redox reactions of O, which can be allocated to the second Li^+ extraction and insertion. To investigate the origin of this phenomenon, X-ray photoelectron spectroscopy (XPS) was employed to study the possible contribution of reversible anionic (O) redox process to the

overall material capacity. The results shown in Fig. 6 reveal that the Fe 2p spectra (both 2p1/2 and 2p3/2) of fully charged LFSO, LFSO/G, and F-LFSO/G (Fig. 6B) corresponding to 1.11, 1.46, and 1.98 Li+ intercalation respectively (Fig. 6A), are almost identical, which suggesting that the Fe valance did not increase beyond 3+. However, the oxygen spectra change significantly with higher lithiation ratio as shown in Fig. 6C. The Si-O-Si peak is moving to lower bonding energy and O22- peak is getting stronger with higher lithiation ratio (from LFSO, to LFSO/G to F-LFSO/G). The XPS results suggests the existence of structure/valence change of O during charge/discharge process. The F-doping helped to stabilize/improve the reversible redox reactions of both Fe (0, 2+, 3+) and O (2-, 1-), consequently, achieved 2-electron transference and theoretical specific capacity. However, more work is needed and in progress to reveal the details of the mechanism of F-doping enabling both cationic and anionic redox reactions.

Table 1. Lattice parameters of Li_2FeSiO_4, $LiFeSiO_4$, and $FeSiO_4$ of this work and referenced work 5.

	This work				Ref. #			
	a, Å	b, Å	c, Å	beta	a, Å	b, Å	c, Å	beta
Li_2FeSiO_4	8.29	5.09	8.32	98.93	8.29	5.09	8.32	98.93
$LiFeSiO_4$	10.1	5.03	6.65	89.08	10.1	5.03	6.65	89.09
$FeSiO_4$	7.18	5.50	9.35	92.75	7.19	5.34	9.32	93.36

To the best of our knowledge, the O redox has been only captured in LFSO based materials at a very slow charge/discharge rate (C/50) with elevated temperature (55 °C), which highly suggests that the O redox is extremely sensitive to the charge/discharge kinetics[28]. In our results, the graphene incorporation greatly increased the charge/discharge capacity (Fig. 1D), and the same results have been observed in our rate performance (Fig. 1C). These results confirm that the kinetics of LFSO have been greatly improved with graphene incorporation. Such argument has been validated in previous literature, in which a high specific capacity of ~320 mAh/g has been reported with those graphene activated LFSO[29-30]. As the consequence, the key point of such phenomenon is that an O redox is activated from the improved kinetics with graphene incorporation while the fluorine doping may change the O boding structure to stabilize this O redox.

To further investigate the tendency of the oxygen redox reaction of our iron rich lithium iron silicate, a spin-polarized density functional theory (DFT) calculations were performed to study its charge transfer mechanism during charge/discharge process. Previously, Zhang et al has systematically studied the structural properties and energetics of Li_2FeSiO_4 polymorphs and their delithiated products[5]. It was concluded that the P21/n space group of Li2FeSiO4 results in the lowest energy compared to other polymorphs. Therefore, similar models were built based on P21/n space group to represent fully lithiated (Li_2FeSiO_4), partially delithiated ($LiFeSiO_4$), and completely delithiated ($FeSiO_4$) polymorphs. The optimized structures are shown in Figure 7. The lattice parameters of these optimized structures are in good agreement with the work by Zhang et al., as shown in Table 1. As indicated by Bader charge analysis, the charge density of Fe and O of the fully lithiated Li_2FeSiO_4 are +1.31 and -1.54 e-, respectively. Compared with fully delithiated material, FeSiO4, the charge density on Fe and O are +1.86 and -1.20 e-. This indicates that during the complete delithiation, or discharge cycle, Fe and O lose similar amount of electrons, the change of electron density are 0.37 and 0.34 e-. More interestingly, based on the charged density of Fe and O in the partially delithiated system ($LiFeSiO_4$), +1.71 and -1.42 e-, Fe lost 0.4 e- while O lost -0.12 e-. It is evident that during the discharge cycle, Fe will get oxidized first, then O will be oxidized, suggesting a potential O redox during LFSO charge/discharge process.

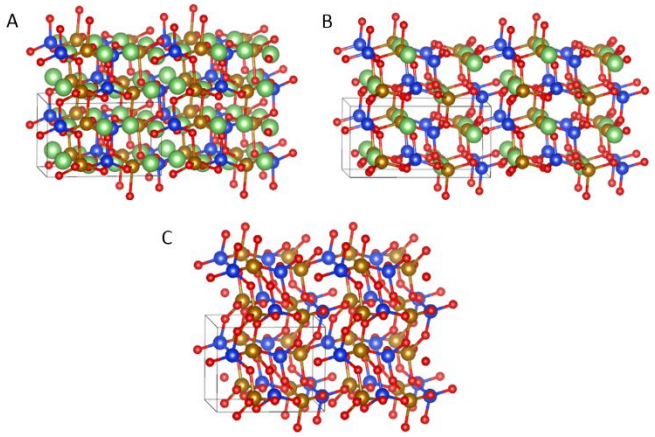

Figure 7. Optimized bulk structures of Li_2FeSiO_4 (A), $LiFeSiO_4$ (B), and $FeSiO_4$ (C). Color code: blue-Si, yellow-Fe, green-Li, and red-O.

3 Conclusion

Fluorine-doped and graphene-incorporated iron rich lithium iron silicate (F-LFSO/G) nanoparticle was synthesized using a simple and effective hydrothermal method. Compare to the blank LFSO, incorporation of graphene into LFSO significantly improves the conductivity. Furthermore, the fluorine doping can stabilize them so that the two-electron process can be realized. As the result, at room temperature under 0.1C, F-LFSO/G delivers a specific capacity as high as 328.43 mAh/g, which is almost 99% of the theoretical specific capacity of Li_2FeSiO_4 (331 mAh/g) and retains 80% initial capacity for more than 40 cycles. The high capacity corresponds to extraction and insertion of two Li+ ions from the orthosilicate host. The redox reaction of O involves in the discharge/charge process is one of the causes of the capacity decay because the peroxide O_2^{2-} is unstable. Although the potential O redox reaction associated with LFSO was investigated by DFT calculations, more work is required to further validate this hypothesis. Considering the simple and energy-efficient synthesis method, the high specific capacity and energy, low cost, and environmental friendliness, the modified lithium iron silicate material, presented here, is a promising candidate as cathode material for next-generation Li-ion batteries.

4 Experimental section

4.1 Materials synthesis

$Li_{4-2x}Fe_xSiO_4$ was synthesized via a hydrothermal method. First, 16 mmol $LiOH{\cdot}H_2O$ (Fisher Chemical, Laboratory Grade) and 3.76 mmol Nano-SiO_2 (Sigma Aldrich, 99.5%) were dissolved in 30 mL distilled water (A). Then, 4 mmol $FeCl_2{\cdot}4H_2O$ (Acros Organcs, 99+%) was dissolved in another 20 mL distilled water (B). After stirring for 1 h, the aqueous solution B was added dropwise into solution A.

Graphene oxide (GO) was synthesized according to our previous method.[21] After stirring for 4 hours, 20 mL pre-prepared GO (5 mg/mL) dispersion was added dropwise into the solution and continued stirring for 1 h. Then, 0.48 mmol NH_4F (Fisher Chemical, >98%) was added into the above mixture and stirred for 5 min before hydrothermal reaction. Finally, the mixture was quickly transferred into a 100 mL Teflon-lined stainless-steel autoclave. After sealing, the autoclave was maintained at 180 °C for 24 h. When the reaction was completed, the autoclave was cooled down to room temperature slowly. The precipitates were washed with DI water for several times and finally dried at 60 °C for 12 hours under vacuum. The pure $Li_{4-2x}Fe_xSiO_{3.76}F_{0.48}$/G (stoichiometric ratio based on precursor materials added to the reaction) was sintered at 600 °C for 10 hours under forming gas (5% H_2 in Ar) atmosphere. Eventually, the sample was collected and labelled as F-LFSO/G. For comparison, we also synthesized the sample without F doping and the blank sample without F-doping with or without graphene-incorporating named LFSO/G, LFSO/blank, respectively.

4.2 Materials characterization

The crystalline structure of the as-prepared sample was characterized using powder X-ray diffraction (XRD), Shimadu XRD-6000 (Shimadu Corporation, Japan) in 2θ range from 10° to 80° with Cu Kα radiation (λ = 0.154 nm). SEM characterization and energy-dispersive X-ray spectroscopy characterization were performed using a JEOL 7800 (JEOL Ltd, Japan) operated at 5 kV. TEM characterization was performed using a JEOL 2100F (JEOL Ltd, Japan) operated at 200 kV. Cyclic voltammetry (CV) was tested using Biologic VMP-30 (Biologic Science Instrument Ltd, France) at a scan rate of 0.2 mV/s with a voltage range of 1.2-4.8 V. In operando HEXRD measurements were performed on the beam line 11-ID-C at Advanced Photon Source, Argonne National Laboratory. The obtained 2D diffraction patterns were calibrated using a standard CeO2 sample and converted to one-dimensional patterns using Fit2D software[31]. In operando XANES measurements during the cycling of coin cells were performed on the beam line 20-BM-B at Advanced Photon Source, Argonne National Laboratory. The XANES data reduction and analysis followed standard methods using the ATHENA software package [32]. XPS characterization was carried out at post test facility at ReCell Advanced Battery Recycling in Argonne National Laboratory.

4.3 Electrochemical performance characterization

The electrochemical performance of prepared F-LFSO/G composites as cathode material was tested by using 2016-type coin cell with Li foil (MTI Corporation) as counter/reference electrode. LiPF6 salt dissolved in a mixture of ethylene carbonate (EC) and ethylene-methyl carbonate (EMC) (EC/EMC = 3:7 by weight) was used as the 1.2 M $LiPF_6$ in EC/EMC electrolyte. LiPF6, EC and EMC were purchased from Novolyte Technologies. A polypropylene microporous film (Celgard 2500, Celgard LLC., North Carolina, USA) was used as the separator. The composite electrode was prepared by mixing active materials, carbon black and poly(vinylidene) fluoride (PVDF, Alfa Aesar) binder with a mass ratio of 8:1:1. Before assemble coin cell in an argon-filled glove box, the electrodes were dried at 65 °C overnight under vacuum. A Solartron 1287A/1260A Potentiostat/Impedance System (Solartron Analytical, England, UK) was used to measure the AC impedance of the cells in the frequency range of 0.01 Hz–1MHz with an amplitude of 5 mV. The electrochemical tests were performed using a multichannel battery testing system (LANHE CT2001A, Wuhan, China) with voltage window of 1.2–4.8 V (versus Li/Li^+) under different current densities at room temperature.

4.4 Computational method details

Spin-polarized density functional theory (DFT) calculations were performed using the Vienna ab initio simulation package (VASP)[33]. The eneralized gradient approxation (GGA)-Perdew-Burke-Ernzerhof (PBE) functional was used to account for the electron exchange-correlation effects[34]. The projector augmented wave (PAW) method was used to treat the ion-electron interactions[35-36]. K-point meshes of 6×6×6 based on the Monkhorst-Pack scheme was used for bulk relaxation[37]. A cut off energy of 520 eV for the plane wave basis set was used for all calculations. The break condition for self-consistent iteration was 1×10^{-6}. Ionic relaxation was stopped when the forces on all atoms are smaller than -0.02 eV/Å. In addition, the localization of d-electrons of iron was corrected using DFT+U approach[38]. The value of Ueff (U-J) was set to be 4 eV, which has been widely used for Fe^{2+}, Fe^{3+}, and Fe^{4+} in the silicate systems[5, 17, 39]. In order to study the charge transfer mechanism, Bader charge analysis was carried out to reveal the charge densities on Fe and O during (de)lithiation [5, 40].

Author Contributions

T. L., Y. L. and J. X. conceived the concepts of this work. T. L., and Y. L. prepared the materials and conducted the electrochemical performance and characterization tests. T.L., Y. L. and Y. Y. prepared the manuscript. Y. R., C. S., W. L. performed and analysed the in-situ XRD and XAS tests, respectively. Y. L. and P. F helped the TEM testing of the materials. The computation calculations were carried by J.Y.X. and C. L. Z. Y. performed the XPS testing for these materials. All the authors participated in the manuscript preparation and discussion.

Conflicts of interest

There are no conflicts to declare.

Acknowledgements

The acknowledgements come at the end of an article after the conclusions and before the notes and references. XAS was performed on Sector 20 facilities at the Advanced Photon Source and research at these facilities are supported by the U.S. Department of Energy - Basic Energy Sciences, the Canadian Light Source and its funding partners, the University of Washington, and the Advanced Photon Source. Use of the Advanced Photon Source and the Center for Nanoscale Materials, Office of Science User Facility, operated for the U.S. Department of Energy (DOE) Office of Science by Argonne National Laboratory, was supported by the U.S. DOE under Contract No. DE-AC02-06CH11357. The authors gratefully acknowledge the help from Post Test Facility at Argonne

National Laboratory, supported by the U.S. DOE Vehicle Technologies office under contract number DE-AC02-06CH11357

Notes and references

1. Yuan, L.-X.; Wang, Z.-H.; Zhang, W.-X.; Hu, X.-L.; Chen, J.-T.; Huang, Y.-H.; Goodenough, J. B., Development and challenges of LiFePO4 cathode material for lithium-ion batteries. *Energy Environ. Sci.* **2011,** *4* (2), 269-284.

2. Wang, Y.; He, P.; Zhou, H., Olivine LiFePO4: development and future. *Energy Environ. Sci.* **2011,** *4* (3), 805-817.

3. Nytén, A.; Abouimrane, A.; Armand, M.; Gustafsson, T.; Thomas, J. O., Electrochemical performance of Li2FeSiO4 as a new Li-battery cathode material. *Electrochemistry Communications* **2005,** *7* (2), 156-160.

4. Arroyo-de Dompablo, M. E.; Armand, M.; Tarascon, J. M.; Amador, U., On-demand design of polyoxianionic cathode materials based on electronegativity correlations: An exploration of the Li2MSiO4 system (M=Fe, Mn, Co, Ni). *Electrochemistry Communications* **2006,** *8* (8), 1292-1298.

5. Zhang, P.; Hu, C. H.; Wu, S. Q.; Zhu, Z. Z.; Yang, Y., Structural properties and energetics of Li2FeSiO4 polymorphs and their delithiated products from first-principles. *Phys Chem Chem Phys* **2012,** *14* (20), 7346-51.

6. Tian, M.; Hu, L.; Huang, Z.; Li, M.; Yang, J.; Wang, Z.; Li, J.; Lin, X.; Mu, S., Tri-phase (1-xy) Li2FeSiO4· xLiFeBO3· yLiFePO4 nested nanostructure with enhanced Li-storage properties. *Chemical Engineering Journal* **2019,** *358*, 786-793.

7. Duan, A.; Qiao, H.; He, M.; Wang, T.; Wang, D.; Wang, T.; Wang, H., Growth of lithium iron silicates nanoplates with high energy facets via polymorphs transition for ehanced lithium-ion extraction/insertion reaction. *Functional Materials Letters* **2021**, 2151015.

8. Rangappa, D.; Murukanahally, K. D.; Tomai, T.; Unemoto, A.; Honma, I., Ultrathin nanosheets of Li2MSiO4 (M = Fe, Mn) as high-capacity Li-ion battery electrode. *Nano Lett* **2012,** *12* (3), 1146-51.

9. Xiong Wen (David) Lou, L. A. A., and Zichao Yang, Hollow Micro - /Nanostructures: Synthesis and Applications. *Adv. Mater.* **2008,** *20*, 3987-4019.

10. Singh, S.; Mitra, S., Improved electrochemical activity of nanostructured Li2FeSiO4/MWCNTs composite cathode. *Electrochimica Acta* **2014,** *123*, 378-386.

11. Huang, X.; Li, X.; Wang, H.; Pan, Z.; Qu, M.; Yu, Z., Synthesis and electrochemical performance of Li2FeSiO4/carbon/carbon nano-tubes for lithium ion battery. *Electrochimica Acta* **2010,** *55* (24), 7362-7366.

12. Zheng, Z.; Wang, Y.; Zhang, A.; Zhang, T.; Cheng, F.; Tao, Z.; Chen, J., Porous Li2FeSiO4/C nanocomposite as the cathode material of lithium-ion batteries. *Journal of Power Sources* **2012,** *198*, 229-235.

13. Naoaki YABUUCHI, Y. Y., Kazuhiro YOSHII, and Shinichi KOMABA, Hydrothermal Synthesis and Characterization of Li2FeSiO4 as Positive Electrode Materials for Li-Ion Batteries. *Electrochemistry Communications* **2010,** *78* (5), 363-366.

14. Haeshin Lee, S. M. D., William M. Miller, Phillip B. Messersmith, Mussel-Inspired Surface Chemistry for Multifunctional Coatings. *SCIENCE* **2007,** *318*, 426-430.

15. Armand, M.; Tarascon, J. M.; Arroyo-de Dompablo, M. E., Comparative computational investigation of N and F substituted polyoxoanionic compounds. *Electrochemistry Communications* **2011,** *13* (10), 1047-1050.

16. Armand, M.; Arroyo y de Dompablo, M. E., Benefits of N for O substitution in polyoxoanionic electrode materials: a first principles investigation of the electrochemical properties of Li2FeSiO4−yNy (y = 0, 0.5, 1). *Journal of Materials Chemistry* **2011,** *21* (27), 10026-10034.

17. Shivani Singh, A. K. R., Raja Sen, Priya Johari, Sagar Mitra, Impact of Cl Doping on Electrochemical Performance in Orthosilicate (Li2FeSiO4)_ A Density Functional Theory Supported Experimental Approach. *ACS Appl Mater Interfaces* **2017,** *9*, 26885-26896.

18. Yang, J.; Zheng, J.; Kang, X.; Teng, G.; Hu, L.; Tan, R.; Wang, K.; Song, X.; Xu, M.; Mu, S.; Pan, F., Tuning structural stability and lithium-storage properties by d-orbital hybridization substitution in full tetrahedron Li2FeSiO4 nanocrystal. *Nano Energy* **2016,** *20*, 117-125.

19. Lui, C. H.; Liu, L.; Mak, K. F.; Flynn, G. W.; Heinz, T. F., Ultraflat graphene. *Nature* **2009,** *462*, 339-341.

20. Matthew J. Allen, V. C. T., and Richard B. Kaner, Honeycomb carbon: a review of graphene. *Chem. Rev.* **2010,** *110*, 132-145.

21. Li, Z. F.; Zhang, H.; Liu, Q.; Sun, L.; Stanciu, L.; Xie, J., Fabrication of high-surface-area graphene/polyaniline nanocomposites and their application in supercapacitors. *ACS Appl Mater Interfaces* **2013,** *5*, 2685-2691.

22. Lu, F.; Zhou, Y.; Liu, J.; Pan, Y., Enhancement of F-doping on the electrochemical behavior of carbon-coated LiFePO4 nanoparticles prepared by hydrothermal route. *Electrochimica Acta* **2011,** *56*, 8833-8838.

23. Ni, J.; Jiang, Y.; Bi, X.; Li, L.; Lu, J., Lithium iron orthosilicate cathode: progress and perspectives. *ACS Energy Letters* **2017,** *2* (8), 1771-1781.

24. Liu, Q.; Li, Z. F.; Liu, Y.; Zhang, H.; Ren, Y.; Sun, C. J.; Lu, W.; Zhou, Y.; Stanciu, L.; Stach, E. A.; Xie, J., Graphene-modified nanostructured vanadium pentoxide hybrids with extraordinary electrochemical performance for Li-ion batteries. *Nat Commun* **2015,** *6*, 6127.

25. Liu, Q.; Liu, Y.; Yang, F.; He, H.; Xiao, X.; Ren, Y.; Lu, W.; Stach, E.; Xie, J., Capacity Fading Mechanism of the Commercial 18650 LiFePO4-Based Lithium-Ion Batteries: An in Situ Time-Resolved High-Energy Synchrotron XRD Study. *ACS Applied Materials & Interfaces* **2018,** *10* (5), 4622-4629.

26. Li, L.; Lun, Z.; Chen, D.; Yue, Y.; Tong, W.; Chen, G.; Ceder, G.; Wang, C., Fluorination - Enhanced Surface Stability of Cation - Disordered Rocksalt Cathodes for Li - Ion Batteries. *Advanced Functional Materials* **2021**, 2101888.

27. Kitchaev, D. A.; Lun, Z.; Richards, W. D.; Ji, H.; Clément, R. J.; Balasubramanian, M.; Kwon, D.-H.; Dai, K.; Papp, J. K.; Lei, T., Design principles for high transition metal capacity in disordered rocksalt Li-ion cathodes. *Energy & Environmental Science* **2018,** *11* (8), 2159-2171.

28. Masese, T.; Tassel, C.; Orikasa, Y.; Koyama, Y.; Arai, H.; Hayashi, N.; Kim, J.; Mori, T.; Yamamoto, K.; Kobayashi, Y., Crystal structural changes and charge compensation mechanism during two lithium extraction/insertion between Li2FeSiO4 and FeSiO4. *The Journal of Physical Chemistry C* **2015,** *119* (19), 10206-10211.

29. Yang, J.; Kang, X.; He, D.; Zheng, A.; Pan, M.; Mu, S., Graphene activated 3D-hierarchical flower-like Li 2 FeSiO 4 for high-performance lithium-ion batteries. *Journal of Materials Chemistry A* **2015,** *3* (32), 16567-16573.

30. Yang, J.; Hu, L.; Zheng, J.; He, D.; Tian, L.; Mu, S.; Pan, F., Li 2 FeSiO 4 nanorods bonded with graphene for high performance batteries. *Journal of Materials Chemistry A* **2015,** *3* (18), 9601-9608.

31. Liu, Q.; He, H.; Li, Z. F.; Liu, Y.; Ren, Y.; Lu, W.; Lu, J.; Stach, E. A.; Xie, J., Rate-dependent, Li-ion insertion/deinsertion behavior of

LiFePO4 cathodes in commercial 18650 LiFePO4 cells. *ACS Appl Mater Interfaces* **2014,** *6*, 3282-3289.
32. Tao, L. Q.; Zhang, K. N.; Tian, H.; Liu, Y.; Wang, D. Y.; Chen, Y. Q.; Yang, Y.; Ren, T. L., Graphene-Paper Pressure Sensor for Detecting Human Motions. *ACS Nano* **2017,** *11* (9), 8790-8795.
33. Kresse, G.; Furthmüller, J., Efficiency of ab-initio total energy calculations for metals and semiconductors using a plane-wave basis set. *Computational materials science* **1996,** *6* (1), 15-50.
34. Perdew, J. P.; Burke, K.; Ernzerhof, M., Generalized gradient approximation made simple. *Physical review letters* **1996,** *77* (18), 3865.
35. Blöchl, P. E., Projector augmented-wave method. *Physical review B* **1994,** *50* (24), 17953.
36. Kresse, G.; Joubert, D., From ultrasoft pseudopotentials to the projector augmented-wave method. *Physical review b* **1999,** *59* (3), 1758.
37. Monkhorst, H. J.; Pack, J. D., Special points for Brillouin-zone integrations. *Physical review B* **1976,** *13* (12), 5188.
38. Dudarev, S.; Botton, G.; Savrasov, S.; Humphreys, C.; Sutton, A., Electron-energy-loss spectra and the structural stability of nickel oxide: An LSDA+ U study. *Physical Review B* **1998,** *57* (3), 1505.
39. Hörmann, N.; Groß, A., Stability, composition and properties of Li 2 FeSiO 4 surfaces studied by DFT. *Journal of solid state electrochemistry* **2014,** *18* (5), 1401-1413.
40. Yu, M.; Trinkle, D. R., Accurate and efficient algorithm for Bader charge integration. *The Journal of chemical physics* **2011,** *134* (6), 064111.